PHYSICS

Iran J Radiol. 2016 July; 13(3):e25491. doi: 10.5812/iranjradiol.25491.

Published online 2016 February 17. **Research Article**

Measuring the Effect of Filters on Segmentation of Developmental Dysplasia of the Hip

Hasan Erdinc Kocer,[1] Kerim Kursat Cevik,[2,*] Mesut Sivri,[3] and Mustafa Koplay[3]

[1]Department of Electronics and Computer Education, Technical Education Faculty, Selcuk University, Konya, Turkey
[2]Department of Computer Programming, Bor Vocational High School, Nigde University, Nigde, Turkey
[3]Department of Radiology, Medical Faculty, Selcuk University, Konya, Turkey

[*]*Corresponding author*: Kerim Kursat Cevik, Department of Computer Programming, Bor Vocational High School, Nigde University, Nigde, Turkey. Tel: +90-3883114527, Fax: +90-3883118437, E-mail: kcevik@nigde.edu.tr

Received 2015 January 06; **Revised** 2015 May 11; **Accepted** 2015 May 13.

Abstract

Background: Developmental dysplasia of the hip (DDH) can be detected with ultrasonography (USG) images. However, the accuracy of this method is dependent on the skill of the radiologist. Radiologists measure the hip joint angles without computer-based diagnostic systems. This causes mistakes in the diagnosis of DDH.
Objectives: In this study, we aimed to automate segmentation of DDH ultrasound images in order to make it convenient for radiologic diagnosis by this recommended system.
Materials and Methods: This experiment consisted of several steps, in which pure DDH and various noise-added images were formed. Then, seven different filters (mean, median, Gaussian, Wiener, Perona and Malik, Lee, and Frost) were applied to the images, and the output images were evaluated. The study initially evaluated the filter implementations on the pure DDH images. Then, three different noise functions, speckle, salt and pepper, and Gaussian, were applied to the images and the noisy images were filtered. In the last part, the peak signal to noise ratio (PSNR) and mean square error (MSE) values of the filtered images were evaluated. PSNR and MSE distortion measurements were applied to determine the image qualities of the original image and the output image. As a result, the differences in the results of different noise removal filters were observed.
Results: The best results of PSNR values obtained in filtering were: Wiener (43.49), Perona and Malik (27.68), median (40.60) and Lee (35.35) for the noise functions of raw images, Gaussian noise added, salt and pepper noise added and speckle noise added images, respectively. After the segmentation process, it was seen that applying filtering to DDH USG images had low influence. We correctly segmented the ilium zone with the active contour model.
Conclusion: Various filters are needed to improve the image quality. In this study, seven different filters were implemented and investigated on both noisy and noise-free images.

Keywords: Ultrasonography, Image Processing, Developmental Dysplasia of the Hip, Filtering

1. Background

Developmental dysplasia of the hip (DDH) or dislocation of the hip is a structural defect, which results in incompatibility between the femoral head and the acetabulum. The prevalence rate of the disease has been determined as 1/3000 in the world but is higher in Japan and in the Mediterranean Basin (1). DDH can be treated successfully with early diagnosis. Delay in diagnosis and treatment can cause the extremities (limbs) to shorten, and claudication and restricted movement disorders, which can lead to functional disabilities. If, it is diagnosed in the neonatal period, the success rate of the treatment is 96% in infants, who can achieve anatomically and radiologically normal development following the treatments (2). In children who have reached the age of walking, there is no chance of conservative treatment and surgery is the only course of action. It is unfortunately impossible to get successful results with surgical treatment in all patients. Even if the surgery is successful, the side effects are too great to be ignored (3).

Determining the incidence of DDH requires examining the abnormal situations where there are differences in the hips, and even then the successful detection of a DDH incidence will depend on the method selected, the level of knowledge of the examiner and the community. The incidence rate based on examining approximately 1000 births was reported to be in the 3 - 4% range. Compared to physical examination, ultrasonography (USG) imaging studies have reported better detection and higher incidence rates (4).

Hip developmental disorders can be successfully de-

tected using USG, and following the detection of the disease, staging and treatment can be planned. Technically, the methods of Graf, Harcke, and Terjes are used (5). USG imaging has become one of the most preferred imaging techniques in today's medical practices, and therefore, is also widely used in the detection of DDH. This wide use is because USG is inexpensive, easily available and comparatively safe to the patients, as well as the operators. It is estimated that one out of every four medical diagnostic image studies in the world involves ultrasonic techniques (5). In addition, because the diagnosis of DDH is carried out in the newborn period, the use of USG in infants also prevents exposure to radiation.

The Graf method is commonly used in the diagnosis of DDH with USG images. Graf is a morphological approach where the anatomical features are assessed in a single image of the hip. To use this method, first, the baby is laid on its side and the transducer is placed parallel to the axis of the body with the specific anatomic landmarks (femoral head and acetabulum). Then, the image is displayed in the standard plane and the morphology is determined by measuring the angles of the hip joint (α and β), as shown in Figure 1. However, the low image quality, in general, makes it difficult for the radiologist to determine the hip joint angles.

The presence of noise in the USG images, leads to image quality degradation and reduction in the ability to achieve successful detection (6). In other words, processing USG images is a difficult and challenging task. Therefore, in order to facilitate image processing, pre-processing filters should be applied to the images. Improving the images by applying filters makes the segmentation process more effective.

There are a few studies regarding computer-aided diagnosis of developmental dysplasia of the hip. Luis-Garcia and Alberola-Lopez studied computer-aided diagnosis of developmental dysplasia of the hip. They tried to segment the acetabulum and femur region from USG images (7-9). Their first work (7) was based on the dynamic shape priors method for segmentation of the nonlinear structure tensor in the tensor domain. They proposed dynamically constructing the shape prior, using the anatomical knowledge as well as the segmentation flow itself. In their study, preliminary data on real images showed promising results (7). In 2006, they presented a segmentation method for the hip joint from three-dimensional (3D) ultrasound data. The Kullback-Leibler distance measurement was used as an intrinsic dissimilarity measure; the energy minimization is performed by estimating the optimal parameters of the sphere and paraboloid that best approximate the femoral head and acetabulum, respectively. Experimental results in this study, over several data volumes, showed this approach to be capable of successfully approximating the anatomy of the hip joint using simple geometrical surfaces (8). In 2007, they presented a novel technique for the analysis of ultrasound images, based on the local estimation of parameter σ of the Rayleigh distribution, which is assumed to model the ultrasound signal. It has been shown that the transformation of the original ultrasound image into the local estimator increases the separability between different regions of interest in the hip joint ultrasound images (9). Han-Yong et al. designed and implemented a computer-aided system for treatment of this disease. In this system, they used a mixture-based partial-volume (PV) algorithm to perform bone segmentation on the patient's computed tomography (CT) or magnetic resonance imaging (MRI) image, then, using 3D reconstruction and display of the segmented image, they easily obtained the quantitative measurement of the acetabular index (AI) and the center-edge angle (CEA), which helped in the clinic diagnosis and treatment (10).

Generally, in diagnosis of dysplasia of the hip joint, the assessment of USG images is performed by the radiologist or operator in real-time. However, in some situations, the real-time images are saved for further assessments. In this study, the saved images were used for researching the filtering effects. On the other hand, this filtering application can be implemented online as well. In our future work, we are planning to improve the online automatic diagnosis system for determining DDH abnormalities on USG devices.

This study is part of the computer-aided diagnostic system of DDH diseases. As a pre-processing of the segmentation of USG images, the effects of various filters were measured by applying them to these images. In our study, seven different filters were applied; mean, median, Gaussian, Wiener, Perona and Malik, Lee and Frost, which are widely known and cited in the literature for their ability to obtain better quality USG DDH images. In addition, various noises were added (speckle, salt and pepper, and Gaussian) to the raw DDH USG images. Then, the peak signal to noise ratio (PSNR) and mean square error (MSE) were measured in order to evaluate the effect of the filters on segmentation. The last stage of our study was testing images on the USG images segmentation method by applying to the active contour method. This segmentation process was aimed to investigate the ilium zone.

2. Objectives

In this study, we aimed for the automatic segmentation of DDH ultrasound images, in order that radiologists can gain convenience in diagnosis by using this recommended system.

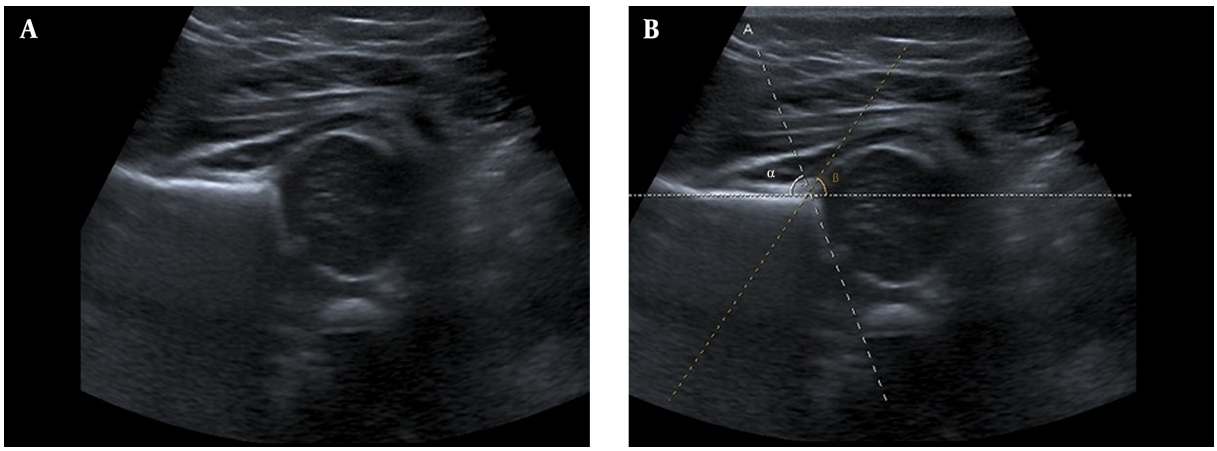

Figure 1. Ultrasonography image for developmental dysplasia of the hip diagnosis. A, Original image; B, Manual selection of α and β angles.

3. Materials and Methods

The raw USG images used in this research were acquired from one device (Toshiba Aplio 400) by one radiologist in the Selcuk university, faculty of medicine, radiology department. These acquired images can differ depending on the probe position and the operator skill. To eliminate the differences caused by having different USG operators, the study uses only one radiologist. The radiologist captures the USG images when he decides to get the best image that can be used for diagnosis of DDH.

The USG images acquired were from infants ranging from 0 - 3 month old (ten anatomically normal babies were randomly chosen), who were laid down laterally onto the table, which had special adaptions used to grasp the baby from both sides in order to keep them still while capturing the image.

This experiment consisted of several steps, in which pure DDH and various noise-added images were formed. Then seven different filters (mean, median, Gaussian, Wiener, Perona and Malik, Lee and Frost) were applied to the images, and finally, the output images were evaluated. The filters used, which are known in the literature, are described in the appendix.

The study initially evaluated the filter implementations on the pure DDH images. Then, three different noise functions; speckle, salt and pepper, and Gaussian were applied to the images and the noisy images were filtered. The main reason of adding these noises to the DDH images was that USG images may have noises for other reasons including the probe, incorrect calibration of the device and environmental effects. In comparison to raw images, these noises added to the DDH images have lower qualities, which can cause an incorrect diagnosis. We have aimed to determine the negative effects of the noises in DDH images. Then, these images were segmented using the active contour model. In the last step, the PSNR and MSE values of the filtered images were evaluated. Figure 2 shows the block diagram of the steps involved in filtering the DDH images.

3.1. Image Quality Measurement

In their diagnosis of DDH, doctors often use the image captured of the right angle and detect the presence of DDH by looking at the femoral and acetabular regions. Therefore, to obtain the best accuracy, the area of the image showing these regions must be clearly displayed. In our work, PSNR and MSE distortion measurements are applied in order to compare the difference in the image quality between the original image and the output image.

Mean square error (MSE) is defined in the following way (6):

$$MSE = \frac{\sum_{i=1}^{M}\sum_{j=1}^{N} x\,(i,j) - x\,(i,j)^2}{MN} \quad (1)$$

where, x (i,j) is the original image, $x\ (i,j)$ is the output image, and MN represents the size of the image.

PSNR is defined in the following manner (6):

$$PSNR = 20log_{10}\left[\frac{(2^n-1)}{\sqrt{MSE}}\right][dB] \quad (2)$$

where, n is the number of bits per pixel used in the image. For a gray-level image, n = 8.

A higher PSNR value of the image indicates that it contains more valuable signals (6). In the same way, a low MSE value shows a lower rate of degradation in the image.

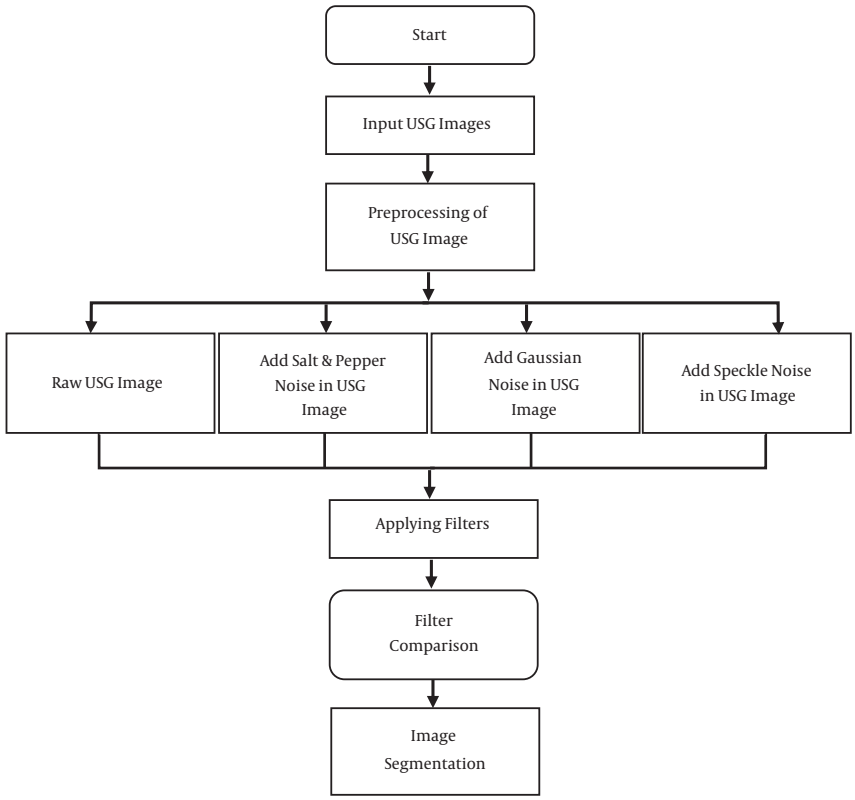

Figure 2. Image processing on developmental dysplasia of the hip (DDH) ultrasonography (USG) image used in this work.

3.2. Image Segmentation Test

The basic idea of the active contour model is to develop curves converging towards the reference object, also known as the general curve fitting method (11-15). The curve to be segmented is selected around the object, and then, according to the effects of the internal and external forces, a converge operation is performed. When displaying the Figure of the resulting curves, the active contour model is divided into two types: open and closed (11, 14, 16-18).

The active contour without edges method is a closed type presented by Chan and Vese (CV) as a successful segmentation algorithm (11). The curve propagation of the algorithm is based on the Mumford-Shah method and level set technique (19). This method is less sensitive to noise than the other contour methods. As in the other contour models, this model also includes a function that minimizes energy levels.

When determining inner lines, the contour moves are not dependent on initial values. This feature distinguishes it from the Snake model. The zero level set of the displayed surface is an active curve, and this curve detects the object in the image. Due to the nature of this closed display, topological changes, such as segmentation and merging, can be detected automatically. In this method, an image is divided into homogeneous regions using this level function. These regions are composed of image parts comprised of closed field values (20).

The CV algorithm defines the F(c_1, c_2, C) energy function for the u_o image, which is divided into two parts with the C closed edge. The function is:

$$\begin{aligned} F(c_1, c_2, C) = \mu, length(C) + \nu, region(in(C)) \\ + \lambda_1 \int_{in(C)} |u_0(x,y) - c_1|^2 dxdy \\ + \lambda_2 \int_{out(C)} |u_0(x,y) - c_2|^2 dxdy \end{aligned} \quad (3)$$

where, $\mu \geq 0$, λ_1, $\lambda_2 > 0$ and are constant parameters, c_1 and c_2 are variables and C are the mean values of the inner and outer regions, respectively. The first term is the regularization term that prevents a small area from merging with the latest detected contour due to noise.

The last two terms are the fitting terms. Using the analysis of the CV level set, the energy function equation is rewritten as (20):

$$F(c_1,c_2,\varphi)=\mu\int_{\Omega}\delta(\varphi(x,y))\,|\nabla\varphi(x,y)|\,dxdy+\nu\int_{\Omega}H(\varphi(x,y))\,dxdy \\ +\lambda_1\int_{\Omega}|u(x,y)-c_1|^2H(\varphi(x,y))\,dxdy+\lambda_2\int_{\Omega}|u_0(x,y)-c_2|^2(1-H(\varphi(x,y)))\,dxdy \tag{4}$$

Equation 5.

while : ϕ: $R^2 \rightarrow R$

$$\varphi(x,t)\begin{cases} x\in\omega\,(in)\rightarrow>0 \\ x\in\partial\omega=C(t)\,(limit)\rightarrow=0 \\ x\in\Omega-\omega\,(out)\rightarrow<0 \end{cases} \tag{5}$$

meets the level set conditions, and H (ϕ) is defined as the Heaviside step function:

$$H(\varphi)=\begin{cases}\varphi\geq 0\rightarrow 1\\ \varphi<0\rightarrow 0\end{cases} \tag{6}$$

In the solution of the considered problem, when the Euler-Lagrange equation is taken into account, the F energy function becomes:

$$\frac{\partial\varphi}{\partial t}=\delta_\epsilon\left[\mu div\left(\frac{\nabla\varphi}{|\nabla\varphi|}\right)-\nu-\lambda_1(u_0-c_1)^2+\lambda_2(u_0-c_1)^2\right]=0 \tag{7}$$

Recursively, it is based on minimization. This equation can only be achieved when the foreground and background information are completely separated from each other (21).

4. Results

In order to carry out the evaluation on the differences in the filters, the filters and noise functions in the study were implemented in MATLAB. Ten images were used in the diagnosis of DDH, and the images were passed through the implemented filters to be evaluated.

The MATLAB command imnoise was used to add the noise to the original images. salt and pepper noise with the variance of σ^2 = 0.02 was added by the command imnoise (img,'salt & pepper',0.02). Gaussian noise with the variance of σ^2 = 0.02 was added by the command imnoise (img,'gaussian',0,0.02) and speckle noise with the variance of σ^2 = 0.05 was added by the command imnoise (img,'speckle',0.05). Then the raw (original) and the noisy images were passed through the seven filters in order to evaluate the performance of the filters.

Two different methods encountered often in the literature were used in this work to carry out the evaluation of the results (6). These are; (a) image quality measurement and (b) image segmentation.

According to the previous research found in the literature regarding image enhancement, PSNR and MSE values are generally taken into account for measuring the image quality. Actually, obtaining the best values of PSNR and MSE for USG images does not mean the best diagnosis in DDH. However, previous works show that in segmentation level, noises in USG images negatively affect the determination of the region of interest. We have investigated the effects of known filters in segmentation of the ilium region located in USG images.

Table 1 shows the results of PSNR and MSE for different image filters of raw images. Based on Table 1, Wiener filtering had the highest average PSNR value (43.49) followed by median filtering and then Frost filtering.

Table 2 shows the results of PSNR and MSE for different image filters of Gaussian noise- added images. Based on Table 2, Perona and Malik filtering had the highest average PSNR value (27.68) followed by mean filtering and then Lee filtering.

Table 3 shows the results of PSNR and MSE for different image filters of salt and pepper noise-added images. Based on Table 3, median filtering had the highest average PSNR value (40.60) followed by mean filtering and Gaussian filtering.

Table 4 shows the result of PSNR and MSE for different image filters of speckle noise- added images. Based on Table 4, Lee filtering had the highest average PSNR value (35.35) followed by Gaussian filtering and then mean filtering.

Based on the PSNR values shown in the tables, it was observed that the Wiener filter removes more noise than other filters for raw images, the median filter removes more noise than other filters for salt and pepper noise-added images, the Perona and Malik filter removes more noise than other filters for the Gaussian noise-added images, and finally, the Lee filter removes more noise than other filters for speckle noise-added images.

The next stage of our study was to test the USG im-

Table 1. PSNR and MSE Values in the Raw Images

Image	Randomly Selected Image		Average Value of 10 Images	
	PSNR	MSE	PSNR	MSE
Frost	40.08	6.38	40.63	5.72
Gaussian	38.56	9.07	39.05	8.20
Lee	38.52	9.14	39.10	8.12
Mean	38.22	9.80	38.71	8.86
Median	40.31	6.06	40.92	5.37
Perona Malik	30.57	56.99	31.12	50.67
Wiener	42.83	3.39	43.49	2.97

Abbreviations: PSNR, peak signal to noise ratio; MSE, mean square error.

Table 2. PSNR and MSE Values in the Images with Gaussian Noise Added[a]

Image	Randomly Selected Image		Average Value of 10 Images	
	PSNR	MSE	PSNR	MSE
Noisy	18.51	915.43	18.51	917.40
Frost	23.62	282.41	23.58	285.21
Gaussian	26.06	161.16	25.97	164.42
Lee	26.02	162.67	25.96	164.82
Mean	26.05	161.54	26.00	163.58
Median	25.25	194.17	25.29	192.56
Perona Malik	27.71	110.12	27.68	111.81
Wiener	24.35	238.98	24.31	241.27

Abbreviations: PSNR, peak signal to noise ratio; MSE, mean square error.
[a] σ^2 =0.02.

Table 3. PSNR and MSE Values in the Images Salt and Pepper Noise Added[a]

Image	Randomly Selected Image		Average Value of 10 Images	
	PSNR	MSE	PSNR	MSE
Noisy	20.93	524.38	20.99	518.20
Frost	26.69	139.23	26.58	142.91
Gaussian	29.99	65.14	29.68	70.01
Lee	29.83	67.56	29.66	70.33
Mean	29.84	67.48	29.68	70.12
Median	41.74	4.35	40.60	5.78
Perona Malik	22.98	327.29	22.93	332.24
Wiener	21.74	435.97	21.74	435.83

Abbreviations: PSNR, peak signal to noise ratio; MSE, mean square error.
[a] σ^2 = 0.02.

age segmentation method by applying the active contour method. This segmentation process is aimed to investigate the ilium.

Firstly, all the images in the ilium were manually seg-

Table 4. PSNR and MSE Values in the Images Speckle Noise Added[a]

Image	Randomly Selected Image		Average Value of 10 Images	
	PSNR	MSE	PSNR	MSE
Noisy	28.62	89.39	28.36	96.71
Frost	33.38	29.89	33.37	30.30
Gaussian	34.97	20.70	35.30	19.37
Lee	34.88	21.15	35.35	19.14
Mean	34.74	21.82	35.20	19.81
Median	32.83	33.86	32.94	33.41
Perona Malik	30.30	60.63	31.26	49.11
Wiener	31.75	43.45	31.63	45.12

Abbreviations: PSNR, peak signal to noise ratio; MSE, mean square error.
[a] $\sigma^2 = 0.05$.

mented, and the center-point was determined. Then the center, right-end and left-end points was identified in the ilium region. Thus, the original image values were created. The process used for the automatic segmentation active contour method was tested in the filtered images (Figure 3). For the automatically segmented image in the ilium, center, right-end and left-end points were determined. To determine the success of the process of segmentation, the measures were compared (Table 5).

According to Table 5, Perona and Malik filtering had the best result (94.17993) as far as closeness to the raw image segmentation coordinate values. In addition, almost all filtering techniques applied in this study had close proximity values.

5. Discussion

In the literature, various methods of noise removal have been proposed and successfully implemented in USG images. The objective of the current study was to evaluate the efficiency of applying filters on USG images in order to increase the rate of DDH detection. Therefore, the study implemented seven different filters and evaluated their efficiency when applied to USG images of pure and noise-added DDH images. A variety of filter configurations was simulated to remove noise, and the results for different filters were obtained. Based on proximity values shown in Table 5, it is observed that filters applied to the DDH images on the segmentation process have low influence. However, in some cases this effect, which appears small, may lead to serious consequences. However, the study concluded that two or three filters should be used together, and that the segmentation method should be used to measure the image quality.

Previous studies have targeted enhancing USG image quality by applying different filters. The success rate of enhancement depends on the probe of the device, the acquirement angle, the noise type in the image, filter parameters and assessment criteria. Therefore, it is not appropriate to compare our study with other studies (22-26).

In our study, it was observed that the Wiener filter removed more noise than other filters for raw images, with the highest average PSNR value (43.49), the median filter removed more noise than other filters for salt and pepper noise-added images, with the highest average PSNR value (27.68), the Perona and Malik filter removed more noise than other filters for Gaussian noise-added images, with the highest average PSNR value (40.60) and finally, the Lee filter removed more noise than other filters for Speckle noise-added images, with the highest average PSNR value (35.35).

When we analyzed the literature regarding segmentation of hip joints, it was seen that all results were reported as promising, but numerical results were not shown. In our study, active contour model-based segmentation was implemented for obtaining the femur region and compared with a manually segmented femur region. As a result of this process, Perona and Malik filtered images segmented properly (7-10).

However, there are limitations as well. From a diagnostic point of view, only the ilium region segmentation was not adequate. After acetabulum region segmentation, angular values (α, β) should be determined in real time. These values should be compared to a radiologist's values. All of these processes must be implemented for computer-aided diagnosis of DDH in real time.

Table 5. Image Segmentation Test Results

Position	Original	Noisy	Frost	Gaussian	Lee	Mean	Median	Perona Malik	Wiener
C	100	96.10803	96.10656	96.12633	96.09667	96.09667	96.13771	95.26996	96.10656
R-E	100	96	96	96	96	96	96	96.39445	96
L-E	100	96.83772	96.83772	96.83772	96.83772	96.83772	96.83772	95.87689	96.83772
C	100	97.07781	97.08108	96.56815	96.54589	96.54589	96.56815	94.7487	97.08725
R-E	100	97.17157	97.17157	97.17157	97.17157	97.17157	97.17157	97.76393	97.17157
L-E	100	98	98	98	98	98	98	96.83772	98
C	100	88.8608	88.87343	88.91621	88.9244	88.89814	88.88991	89.90939	88.93951
R-E	100	87.95841	87.95841	87.19375	87.19375	87.19375	87.19375	90	87.95841
L-E	100	98	98	98	98	98	98	98	98
C	100	90.07169	90.62597	90.69148	90.63807	90.66238	90.96999	92.09718	90.08143
R-E	100	84.9667	84.9667	84.9667	84.9667	84.9667	84.9667	95.75736	84.9667
L-E	100	98.58579	98.58579	98.58579	98.58579	98.58579	98.58579	98.58579	98.58579
C	100	96.88377	96.90905	96.89839	96.89839	96.89839	96.89642	97.23204	96.90373
R-E	100	95.87689	95.87689	95.87689	95.87689	95.87689	95.87689	95.87689	95.87689
L-E	100	97	97	97	97	97	97	97	97
C	100	92.92745	92.71752	92.63755	92.59781	92.60756	92.66727	92.57644	92.80749
R-E	100	94.34315	94.34315	94.34315	94.34315	94.34315	94.34315	94.34315	94.34315
L-E	100	89.95012	89	89	89	89	89	87.95841	89.95012
C	100	92.59265	92.61307	92.61307	92.63305	93.12715	92.60307	92.01797	92.68256
R-E	100	95.52786	95.52786	95.52786	95.52786	95.52786	95.52786	96.39445	95.52786
L-E	100	89	89	89	89	89	89	87	88.95464
C	100	89.53652	89.57676	89.5965	89.60675	89.60675	89.49678	90.12975	89.61622
R-E	100	97.17157	97.17157	97.17157	97.17157	97.17157	97.17157	95.75736	97.17157
L-E	100	92	92	92	92	92	92	92	92
C	100	96.60975	96.60864	96.56889	96.45846	96.45846	96.47722	96.17772	96.60751
R-E	100	98	98	98	98	98	98	97.76393	98
L-E	100	93.91724	93.91724	93.91724	93.91724	93.91724	93.91724	92.92893	93.91724
C	100	93.90882	94.01421	93.98027	93.98027	93.98027	93.93195	93.66972	94.04815
R-E	100	95.87689	95.87689	95.87689	95.87689	95.87689	95.87689	95.52786	96.39445
L-E	100	93	91.456	91.456	91.456	91.456	91.75379	89.80196	91.05573
Average	100	94.12537	94.06054	94.0174	94.01016	94.02689	94.02871	94.17993	94.08641

Abbreviations: C, Center; R-E, Right-End; L-E, Left-End.

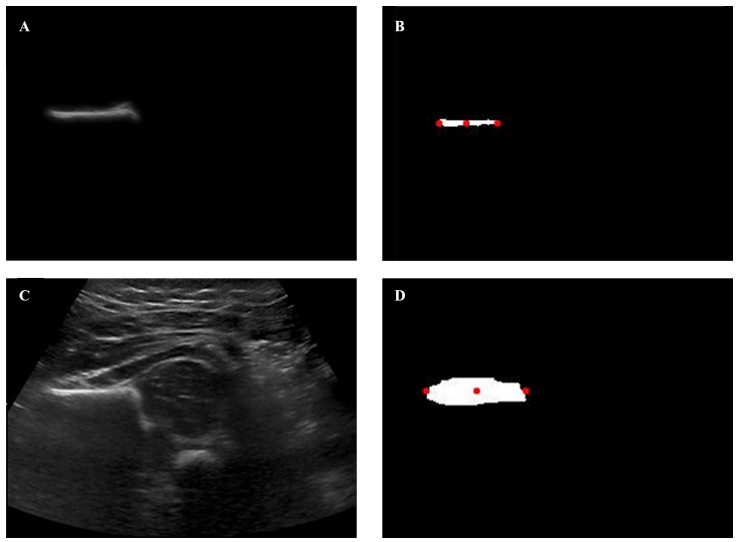

Figure 3. DDH image. A, Manually segmented image; B, Manually segmented image binary for C,R-E,L-E points; C, Raw image; D, Automatically segmented image binary for C,R-E,L-E points (C, Center; R-E, Right-End; L-E, Left-End).

Acknowledgments

This study was carried out in Selcuk university, department of computer engineering as a doctoral thesis.

Footnotes

Authors' Contribution: The study was carried out as a part of a doctoral thesis. Hasan Erdinc Kocer, the author of the paper, is the PhD supervisor. Kerim Kursat Cevik, the second author of paper, is the PhD student. Mesut Sivri and Mustafa Koplay, the third and fourth authors of paper, provided USG. They work as experts to determine the ilium and femur points.

Financial Disclosure: There has been no fund as a support for the study. In addition, the authors of this study do not expect any financial interests.

Funding/Support: DDH Images were obtained from Selcuk university, faculty of medicine, radiology department.

References

1. Atalar H, Yavuz OY, Uras I, Gunay C. , Saylı U. . Frequency of Evaluation of Developmental Hip Dysplasia Screening Program in Turkey. *Turkey Clinics J Med Sci.* 2008;**28**:357–60.
2. Tosun HB, Bulut M, Karakurt L, Belhan O, Serbest S. Evaluation of the Results of Hip Ultrasonography which Applied for Screening of Developmental Hip Dysplasia. *Fırat Med J.* 2010;**15**(4):178–83.
3. Song KM, Lapinsky A. Determination of hip position in the Pavlik harness. *J Pediatr Orthop.* 2000;**20**(3):317–9. [PubMed: 10823597].
4. Rosendahl K, Markestad T, Lie RT. Ultrasound screening for developmental dysplasia of the hip in the neonate: the effect on treatment rate and prevalence of late cases. *Pediatrics.* 1994;**94**(1):47–52. [PubMed: 8008537].
5. Herring JA. In: Tachdjian's Pediatric Orthopaedics. Herring JA, editor. ; 2003. pp. 513–34.Developmental Dysplasia of the Hip.
6. Wan MH, Supriyanto E. Comparative evaluation of ultrasound kidney image enhancement techniques. *Int J Comput Appl.* 2011;**21**(7):15–9.
7. De Luis-Garcia R, Alberola-Lopez C, editors. Hip joint segmentation from 2D ultrasound data based on dynamic shape priors. Proceedings of the 4th WSEAS international conference on Electronics, control and signal processing. 2005; World Scientific and Engineering Academy and Society (WSEAS); pp. 245–50.
8. De Luis-Garcia R, Alberola-Lopez C, editors. Parametric 3D Hip Joint Segmentation for the Diagnosis of Developmental Dysplasia. Engineering in Medicine and Biology Society, 2006. EMBS '06. 28th Annual International Conference of the IEEE. 2006; pp. 4807–10.
9. Luis-Garcia R, Aja-Fernandez S, Cardenes-A R, Martin-Fernandez M, Alberola-Lopez C, editors. Application to the Diagnosis of Developmental Dysplasia of the Hip. Analysis of Ultrasound Images Based on Local Statistics. 2007; New York. IEEE Ultrasonics Symposium.; pp. 2531–4.
10. Han-Yong C, Xin L, Hong-Bing L, Shu-Yi W, Xiu-Zhen D, editors. Application of Segmentation and Measurement in the Treatment of Developmental Dysplasia of the Hip. Bioinformatics and Biomedical Engineering, 2007. ICBBE 2007. The 1st International Conference on. 2007; Wuhan. IEEE; pp. 989–91.
11. Chan TF, Vese LA. Active contours without edges. *IEEE Trans Image Process.* 2001;**10**(2):266–77. doi: 10.1109/83.902291. [PubMed: 18249617].
12. Sapiro G. Geometric partial differential equations and image analysis. Cambridge: Cambridge university press; 2006.
13. Longest PW, Tian G. Transient absorption of inhaled vapors into a multilayer mucus–tissue–blood system. *Anns of biomed eng.* 2010;**38**(2):517–36.
14. Xu C, Prince JL. Snakes, shapes, and gradient vector flow. *IEEE Trans Image Process.* 1998;**7**(3):359–69. doi: 10.1109/83.661186. [PubMed: 18276256].

15. Chan TF, Sandberg BY, Vese LA. Active Contours without Edges for Vector-Valued Images. *J Vis Commun Image Representation.* 2000;**11**(2):130–41. doi: 10.1006/jvci.1999.0442.
16. Chesnaud C, Refregier P, Boulet V. Statistical region snake-based segmentation adapted to different physical noise models. *IEEE Trans Pattern Anal Mach Intell.* 1999;**21**(11):1145–57. doi: 10.1109/34.809108.
17. Li C, Xu C, Gui C, Fox MD, editors. Level set evolution without re-initialization: a new variational formulation. Computer Vision and Pattern Recognition, 2005. CVPR 2005. IEEE Computer Society Conference on. 2005; IEEE; pp. 430–6.
18. Suri JS, Liu K, Singh S, Laxminarayan SN, Zeng X, Reden L. Shape recovery algorithms using level sets in 2-D/3-D medical imagery: a state-of-the-art review. *IEEE Trans Inf Technol Biomed.* 2002;**6**(1):8–28. [PubMed: 11936600].
19. Osher S, Sethian JA. Fronts propagating with curvature-dependent speed: Algorithms based on Hamilton-Jacobi formulations. *Journal of Computational Physics.* 1988;**79**(1):12–49. doi: 10.1016/0021-9991(88)90002-2.
20. Tunali I, Kilic E, editors. Mass segmantation on mammograms using active contours. Signal Processing and Communications Applications Conference (SIU), 2013 21st. 2013; Girne. pp. 1–4.
21. Narayanan SK, Wahidabanu RSD. A view on despeckling in ultrasound imaging. *Int J Signal Processing.* 2009;**2**(3):85–98.
22. Loupas T, McDicken WN, Allan PL. An adaptive weighted median filter for speckle suppression in medical ultrasonic images. *Circuits and Sys, IEEE Trans on.* 1989;**36**(1):129–35.
23. Mahmood NH, Razif MR, Gany MT. Comparison between median, unsharp and wiener filter and its effect on ultrasound stomach tissue image segmentation for pyloric stenosis. *Inte J Appl Sci Technol.* 2011;**1**(5).
24. Sarode MV, Deshmukh PR. Reduction of speckle noise and image enhancement of images using filtering technique. *Int J AdvancTechnol.* 2011;**2**(1):30–8.
25. Thangavel K, Manavalan R, Aroquiaraj IL. Removal of speckle noise from ultrasound medical image based on special filters: comparative study. *ICGST-GVIP J.* 2009;**9**(3):25–32.
26. Young IT, van Vliet LJ. Recursive implementation of the Gaussian filter. *Signal Processing.* 1995;**44**(2):139–51. doi: 10.1016/0165-1684(95)00020-E.